Impact of Air-Sea Interactions on Extra-Tropical Cyclones

P. Ola G. Persson[1], J. E. Hare[1], L. B. Nance[2], and B. Walter[3]

[1]CIRES/NOAA/ESRL/PSD3, Boulder, CO 80305 USA
[2]National Center for Atmospheric Research, Boulder, CO 80307 USA
[3]Bernard Walter Consulting, Seattle, WA 98101 USA

1. Introduction

Cyclone morphology, life cycle, and associated thermodynamic processes are important for determining the impact of surface fluxes of heat, moisture and momentum on mid-latitude cyclones. Furthermore, the timing and spatial relationships between the storms and the surface fluxes are related to spatial and temporal variations of the ocean surface characteristics, such as sea-surface temperature (SST), wave-height, wave-age, and perhaps even wave orientation. While the main fluxes to be discussed are the sensible and latent heat fluxes and the momentum flux, the representation of these fluxes depend on the proper representation of physical processes, such as wave structure and sea spray. Assessing or representing the impact of air-sea interaction on extratropical cyclones must consider all of these issues.

This paper will provide a synopsis of current knowledge of how air-sea interaction phenomena impact mid-latitude cyclones. It will use previous studies as examples, augmenting these with some previously unpublished material. Suggestions for areas of continued research will be made. Because only the key points of the numerous topics can be discussed, a lengthy bibliography is provided for further study.

2. Surface Flux Impacts

2.1. Impact of surface fluxes and flux timing

Various studies, most relying on numerical models, have shown that the degree to which surface sensible heat and moisture fluxes affect storm evolution and precipitation depends on the location and timing of these fluxes relative to the cyclone and its associated structures. Studies suggest that surface heat and moisture fluxes during a storm's rapid deepening stage produce only modest or no impacts on the storm development and precipitation (Kuo and Reed 1988; Kuo et al. 1991; Reed and Simmons 1991; Kristjánsson and Thorsteinsson 1995), while fluxes occurring before the rapid deepening stage produce larger impacts (Reed and Albright 1986; Kuo et al., 1991; Zhang et al., 1999; Gyakum and Danielson 2000).

In the study by Kuo et al. (1991), surface energy fluxes occurring during the 24-h rapid deepening stage had a minimal impact on the storms' central pressure by the end of the 24-h period and only increased the precipitation by about 25% (Figs. 1a and 2a). This precipitation increase was almost entirely due to the increase of the water vapor supply with little due to changes in energy. When the simulations and the modifications to the surface fluxes were started 24 h earlier, removing the surface energy fluxes increased the central pressure by 12 mb and the precipitation was reduced by 50% (Figs. 1b and 2b). When the energy fluxes were removed for only 24 h of the 48-h simulation, a much larger impact was seen on the storm development when the fluxes were removed for the first 24 h compared to the last 24 h. Hence, the relative timing of the surface fluxes and the storm evolution played an important role in the magnitude of the impact of the surface energy fluxes.

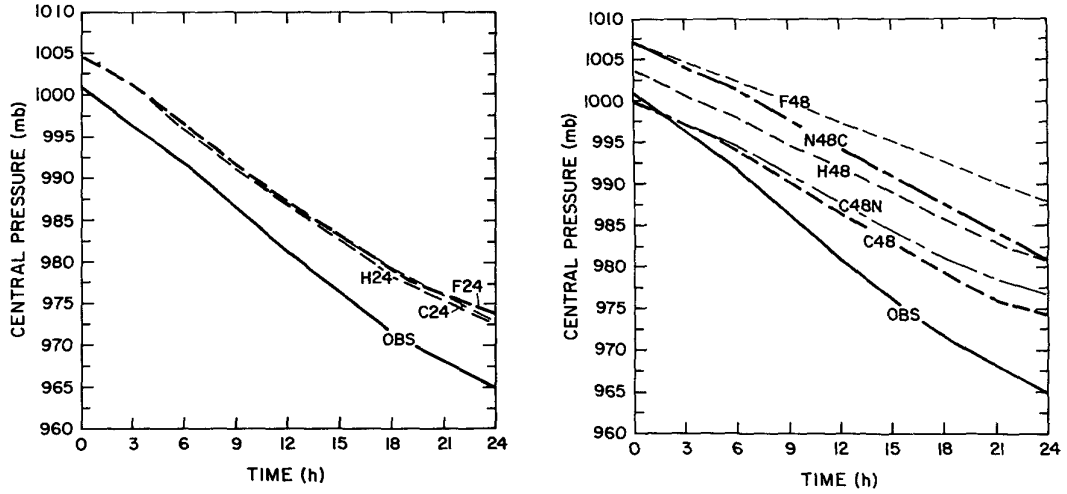

Figure 1: Time series of the observed (OBS) and predicted central pressure averaged over seven western Atlantic Ocean cases during the 24-h explosive development stage when the model fluxes are modified at a) t = 0 h (24 h simulation) and b) t = -24 h (48 h simulation). The experiments are: C24, C48-control runs; H24, H48 - no sensible heat flux; F24, F48 - no energy fluxes; C48N - no energy fluxes last 24 h; N48C - no energy fluxes first 24 h. The MM4 model used a horizontal resolution of 80 km, the Blackadar PBL scheme (Anthes et al 1987), and the modified Arakawa-Schubert convective scheme (Grell et al. 1990). (From Kuo et al. 1991).

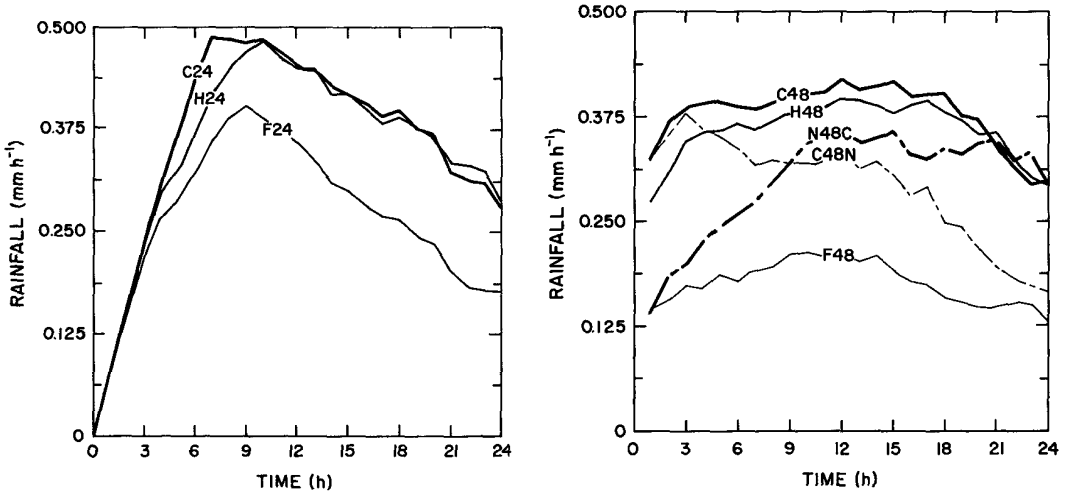

Figure 2: Same as Fig.1, but showing the hourly precipitation rate averaged over the 1600 km x 1600 km region centered on the surface low (From Kuo et al. 1991).

2.2. Impact of different flux schemes

While it is important to understand the impact of including or omitting surface fluxes on the evolution of extratropical cyclones, all numerical models have some type of surface flux scheme. Hence, the more practical issue is whether the surface-flux magnitude variability produced by the primary surface flux schemes has significant impact on the evolution of extratropical cyclones. Furthermore, surface flux schemes in models are generally incorporated into specific planetary boundary layer (PBL) schemes, with the former providing the direct link between the atmosphere and the surface and the latter redistributing the momentum, sensible heat and moisture in the vertical. Though model experiments using different PBL schemes are useful, one must recognize that both the surface flux schemes and the method of vertical redistribution of momentum and energy are being varied.

Persson et al. (2003) performed such a PBL/surface flux sensitivity test using Penn State/NCAR Mesoscale Model (MM5, modified version 3-5) simulations of a decaying cyclone and three frontal waves (called W0, W1, W2, and W3, in Fig. 3) for IOP1 of the Fronts and Atlantic Storm-Track Experiment (FASTEX; Joly et al. 1999). The PBL schemes considered in this study were called BLK (Blackadar 1976, 1979; Zhang and Anthes 1982), MRF (Hong and Pan 1996), BKT (Burk and Thompson 1989), and GYS (Shafran et al. 2000). The first two are first-order schemes and the last two are second order schemes, and include a prognostic equation for the turbulent kinetic energy. The surface flux schemes in the BLK, MRF, and GYS PBL schemes are similar and are based on the Richardson-number dependent parameterization developed by Blackadar (1976, 1979) and described by Grell et al. (1994). The surface flux scheme in the BKT PBL scheme is based on the parameterization by Louis (1979).

The simulations were initialized at 12 UTC Jan. 7, 1997, and run for 84 h until 00 UTC Jan. 11, thereby allowing ample time for the surface fluxes to affect the cyclone evolution. Note that frontal wave W1 was barely noticeable near the east coast of North America at the initialization time, while the perturbation that was to become W2 was over the eastern United States (Fig. 3a). Initial and boundary conditions were provided by European Center for Medium-Range Weather Forecasting (ECMWF) analyses enhanced with surface and rawinsonde observations, including special FASTEX observations. Point and spatial validation were provided by observations from the *R/V Knorr* (Persson et al. 2003, 2005a) and analyses from the French ARPEGE and the ECMWF forecasting systems, respectively.

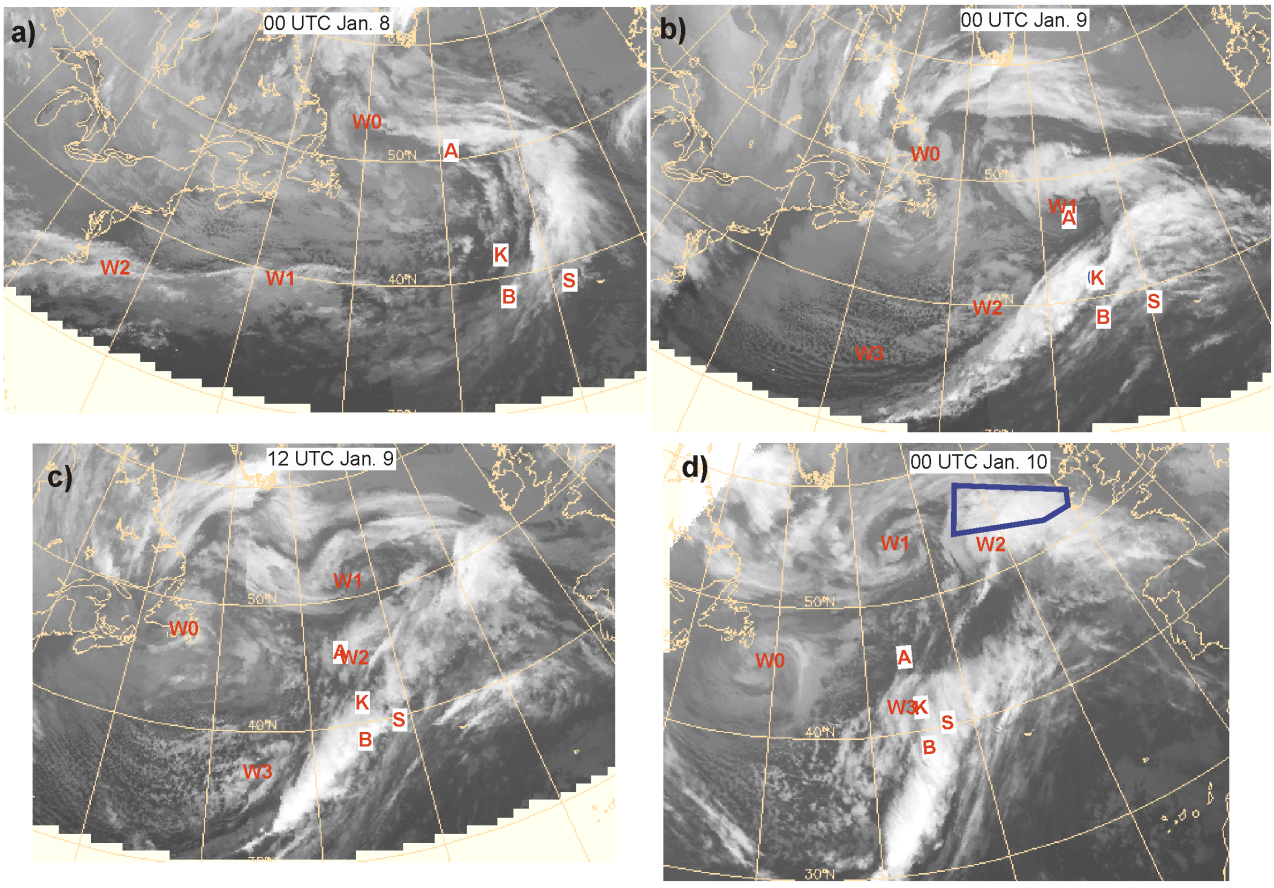

Figure 3: Satellite IR mosaics for a) 00 Z Jan. 8, b) 00 Z Jan. 9, c) 12Z Jan. 9, and d) 00Z Jan. 10, 1997. The positions of the 4 frontal waves, W0-W3 are shown. The locations of the FASTEX research ships Knorr, *(K),* Suroit *(S),* Victor Bugaev *(B), and* Aegir *(A) are shown in each pane. The downstream mesoscale sampling area (MSA) where wave W2 was sampled by three aircraft is shown enclosed in blue in d). (From Persson et al. 2003)*

FASTEX IOP1 consisted of a large cyclone in the central North Atlantic Ocean and three frontal waves. Tracks of all of the waves were just on the warm side of the large SST gradient between the cold Labrador Current and the relatively warm Atlantic Gulfstream (Fig. 4). Wave W1 showed the greatest deepening (Fig. 5b), and downstream mesoscale sampling area measurements of IOP1 were focused on wave W2 (Fig. 3d).

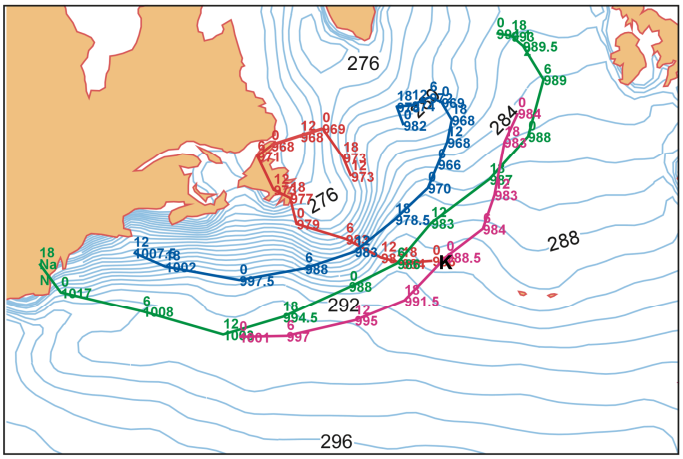

Figure 4: Tracks of the low-pressure center for waves W0 (red), W1(blue), W2 (green), and W3 (magenta) as given by the ECMWF analyses and IR satellite images between 12 UTC Jan. 7 and 00 UTC Jan. 11, 1997. Each 6 hourly location is marked with the hour and central pressure (hPa). Also shown are the surface temperature (K) analysis at 12 UTC Jan. 7 used in the MM5 simulations and the location of the R/V Knorr *(black "K"). (Adapted from Persson et al. 2003)*

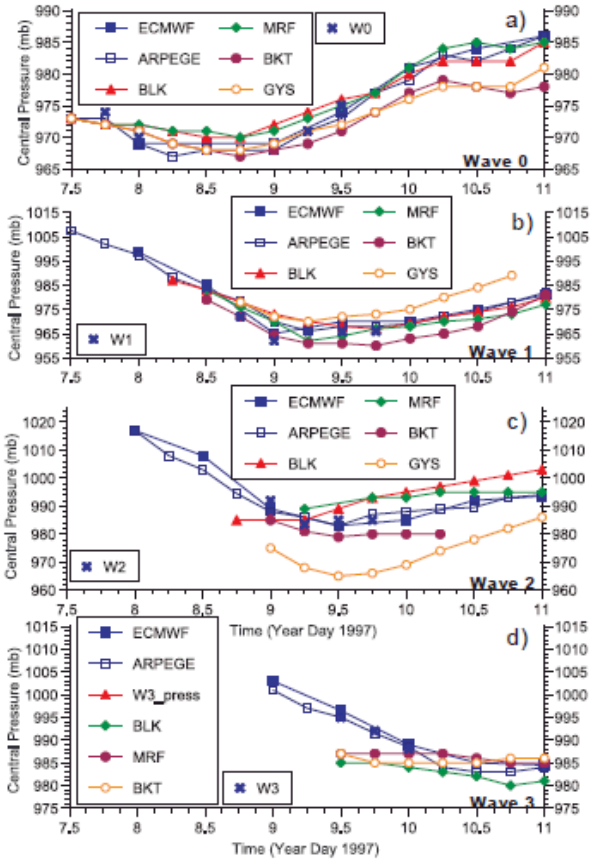

Figure 5: Evolution of the central pressure in the ECMWF and ARPEGE analyses (blue), manual analyses of surface observations ("x"), and the model runs with the four different PBL schemes for a) wave 0, b) wave 1, c) wave 2 and d) wave 3. (From Persson et al. 2003)

However, the entire sequence of waves and their respective developments are important. Observations at the *R/V Knorr* showed that waves W1 and W2 had the classical open-wave, frontal signatures, while W3 passed directly over the *Knorr* and showed a more occluded structure (Fig. 4; also see Persson et al. 2003). Surface fluxes at the *Knorr* were strongly modulated by the synoptic and surface environment, with warm sector regions showing large surface stresses of 0.6-1.2 N m^{-2}, sensible heat fluxes of -50 - +10 W m^{-2}, and latent heat fluxes of 50-150 W m^{-2}. In the post-frontal regions, the stresses were substantially less but the sensible and latent heat fluxes increased by 50-150 Wm^{-2}.

The MM5 simulations were able to replicate the presence of the frontal waves, but using different PBL schemes produced different evolutions. None of the simulations were able to produce the correct track and central pressure for all three waves (Figs. 5 and 6). Of the four PBL schemes considered in this study, the evolution of W1-W3 in the MRF simulation was, for the most part, the best match to the observed behavior of the three waves. Varying the PBL scheme had the largest impact on the evolution of waves W1 and W2. The track of W1 was well replicated only in the MRF simulation, whereas subtle timing issues point to the MRF simulation as being slightly better than the BLK simulation for W2 as well (Fig. 6). The BKT and GYS simulations exhibited very similar erroneous tendencies for the tracks of W1 and W2, suggesting a problem common to these two second-order PBL schemes. The BLK and MRF schemes both replicated the evolution of the central pressures of W0 and W1 reasonably well, while MRF represented the central pressure magnitude of W2 better than any other scheme (Fig. 5).

Varying the PBL schemes (including surface flux schemes) produced differences in cyclone positions of up to 1000 kms (e.g, BLK and GYS for W1) and in the central pressure of up to 30 mb (MRF and GYS for W2), with additional differences in the timing of the wave developments. Because the surface flux schemes in PBL schemes MRF, BLK, and GYS are the same, the differences between simulations MRF, BLK, and GYS are likely due to differences in the PBL portion of the scheme (i.e., vertical redistribution) rather than in the surface fluxes. Since the two second-order PBL schemes (GYS and BKT) produced similar errors despite having different surface flux schemes also suggests that differences between surface flux schemes have less of an impact on the observed sensitivities than the differences in the PBL portion of the schemes.

3. Off-line Flux Evaluations

Though the previous section highlighted the differences obtained with different PBL schemes, it also illustrates the difficulties in doing evaluations of surface flux schemes within the context of a 3-D atmospheric model. Unless care is taken that each model is identical in every way except for the surface flux scheme, a quantification of the effects of different flux schemes is not possible. Furthermore, if comparing to observed fluxes, validation of fluxes from flux schemes is not possible unless one can verify that the bulk atmospheric and surface parameters (e.g., wind speed, air-sea temperature differences, etc.) in the model are the same as in the observations. Hence, off-line validation of surface flux schemes is often preferable to in-model validation. For off-line validations, the observed bulk atmospheric and surface parameters, coincident with the observed surface fluxes, are available as input to the surface flux parameterization schemes.

Data sets used for off-line validation of flux schemes to be used in simulations of extratropical cyclones must contain measurements in the environmental conditions appropriate for extratropical cyclones. In particular, maritime extratropical cyclones occasionally contain regions where the wind exceeds 30 m s^{-1}. Hence, appropriate measurements in high-wind speed, open ocean environments are required. Only a few data sets exist that can meet this criterion.

Brunke et al. (2003) tested 12 different surface flux parameterization schemes using data from 12 maritime tropical and midlatitude measurement programs, including FASTEX and CATCH (Eymard et al. 1999) which had measurements in winds up to 30 m s^{-1}. The parameterization schemes are evaluated for their

ability to reproduce the observed momentum, sensible heat and latent heat fluxes. The four least problematic of the 12 algorithms based upon the overall ranking for this data include the Coupled Ocean–Atmosphere Response Experiment (COARE) version 3.0, the University of Arizona (UA) schemes, that used at the ECMWF, and that at the National Aeronautics and Space Administration (NASA) Data Assimilation Office for version 1 of the Goddard Earth Observing System reanalysis (GEOS-1). Only the COARE scheme was ranked in the top 4 schemes for each of the three flux categories. The ECMWF scheme was problematic for the latent heat flux, while the GEOS-1 scheme was problematic for the wind stress. The UA scheme showed only an average performance for the sensible heat flux. The COARE surface flux scheme is based upon the Liu et al. (1979) algorithm; the ECMWF scheme is based on the work by Beljaars (1995a,b).

Off-line evaluations of the BLK and COARE schemes using FASTEX data (Persson et al. 2003) found that the BLK scheme performed slightly better for stresses greater than 0.4 N m^{-2}, but that it overestimated H_s and, especially, H_l, while the COARE scheme had only minor biases (Fig. 7). The better performance by BLK for τ at high wind speeds can probably be traced to the use of a Charnock constant of 0.032 compared to 0.018 in COARE. Including wave- slope (Taylor and Yelland 2001) and wave-age (Oost et al. 2001, but with an exponent of 4.6 rather than 4.5) parameterization options in COARE provided improvements to τ for high wind speeds, with the accuracy for τ then surpassing that of the BLK scheme (Fig. 7a). The poorer performance of the BLK scheme for H_s and H_l is probably due to that the thermal and moisture surface roughnesses (z_T and z_Q) are set equal to that for momentum (z_0) and that a bulk Richardson number formulation for stability is used to circumvent the need for iteration.

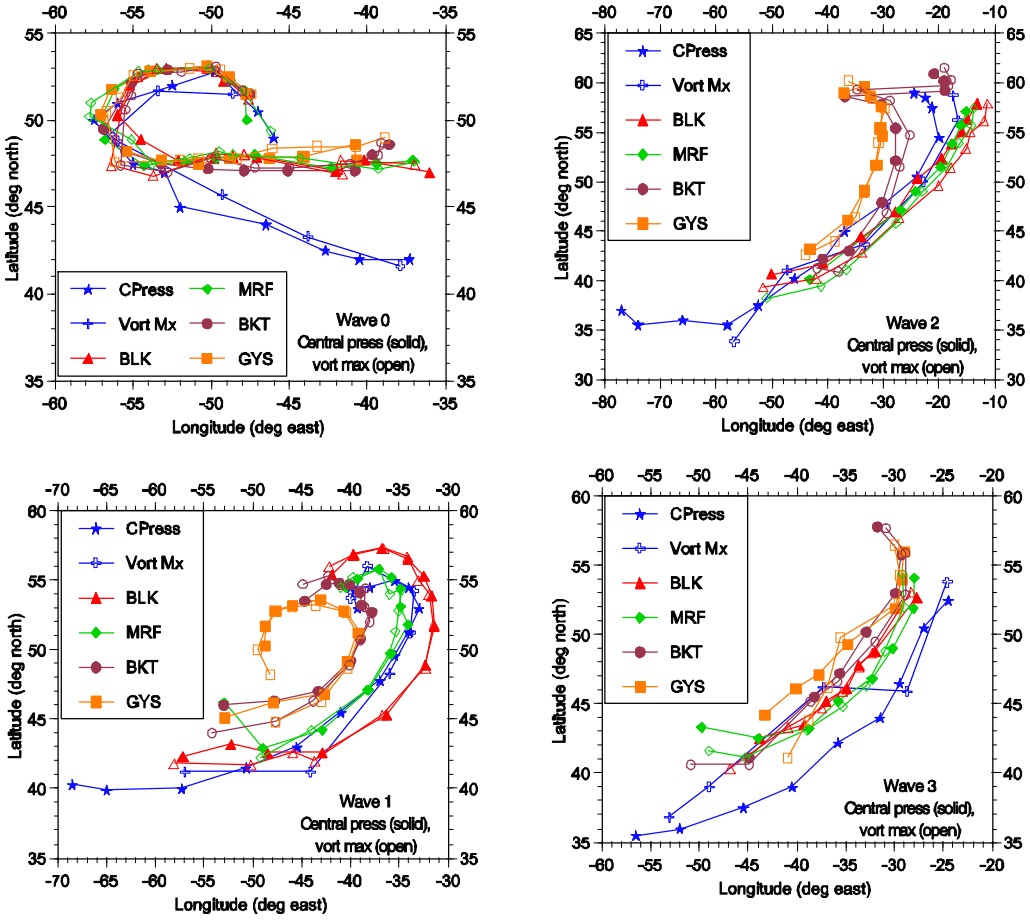

Figure 6: Tracks of the observed (blue) and modeled frontal waves of FASTEX IOP1 using different PBL schemes for a) wave 0, b) wave 1, c) wave 2, and d) wave 3. The tracks are defined by the location of the low-pressure center (solid symbol) and the 925 mb vorticity maximum (open symbol) (Persson et al 2003).

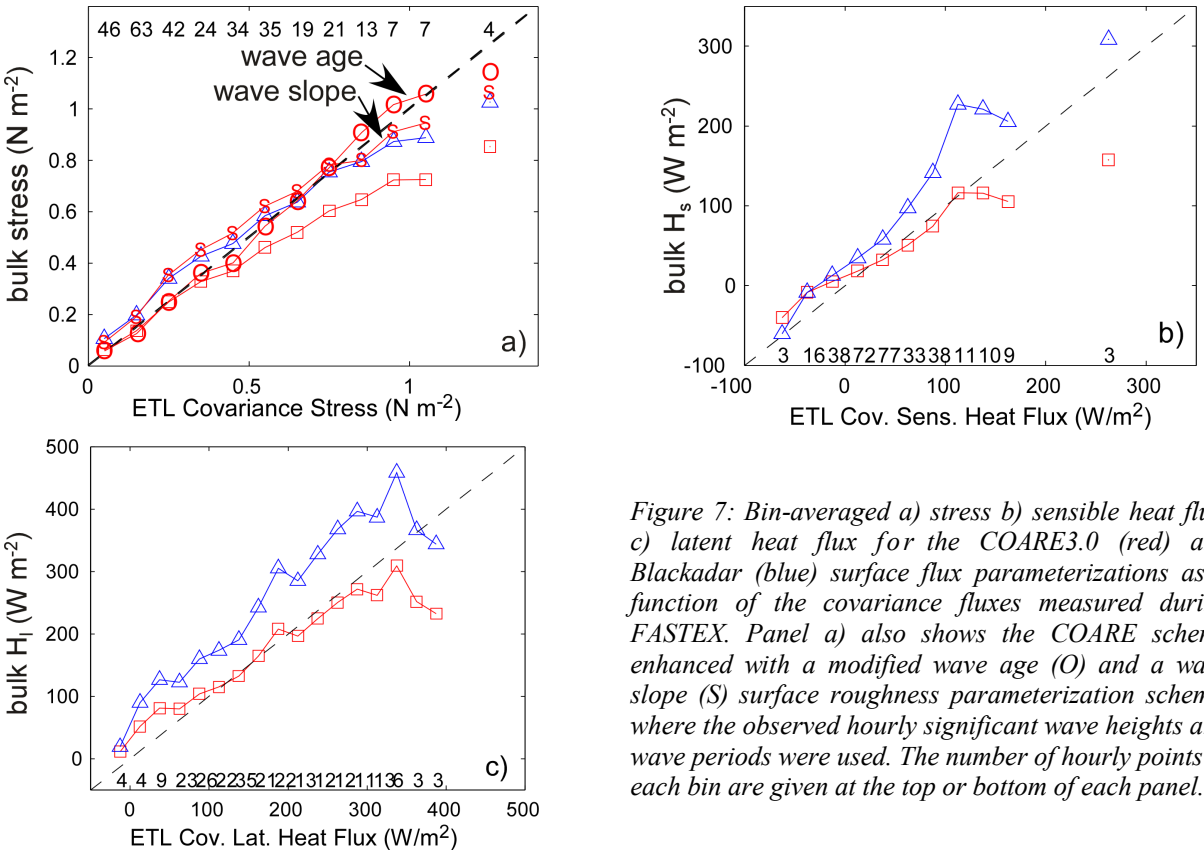

Figure 7: Bin-averaged a) stress b) sensible heat flux, c) latent heat flux for the COARE3.0 (red) and Blackadar (blue) surface flux parameterizations as a function of the covariance fluxes measured during FASTEX. Panel a) also shows the COARE scheme enhanced with a modified wave age (O) and a wave slope (S) surface roughness parameterization scheme, where the observed hourly significant wave heights and wave periods were used. The number of hourly points in each bin are given at the top or bottom of each panel.

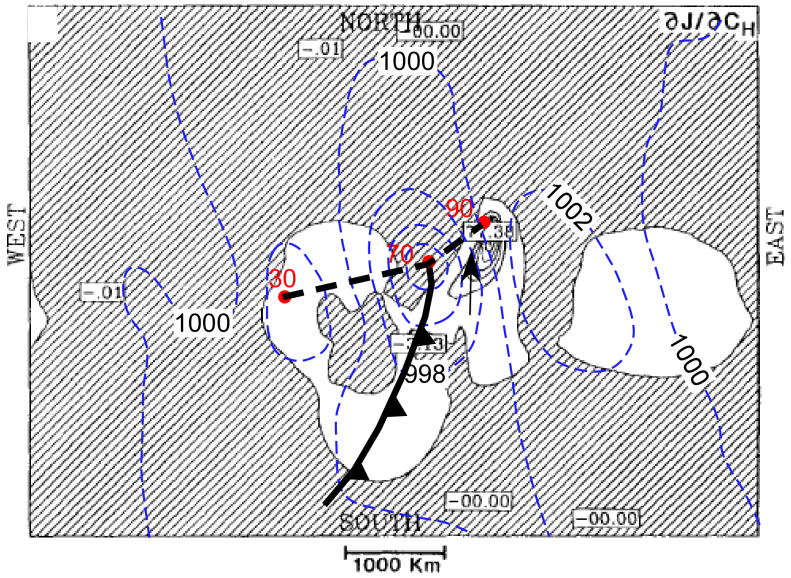

Figure 8: Field of sensitivity to surface heat-transfer coefficient, $\partial J/\partial C_H$, (isopleth = 10 hPa) accumulated between 60 and 90 h. Positive $\partial J/\partial C_H$ indicates H_s is anticyclogenetic for 90 h central pressure. Negative values are hatched. Blue dashed isopleths show surface pressure at 70 h. Red dots show location of low at 30 h, 70 h, and 90 h in this non-linear forecast with sea-surface-temperature anomaly. Heavy dashed line shows the low center track. The approximate location of the surface front and a low-level, warm sector wind vector are also depicted. J is the cost function for the adjoint model. Adapted from Langland et al (1995).

4. Key Flux Regions of Extratropical Cyclones

The location of the surface fluxes relative to the location of the storm and its associated dynamical features also plays an important role. For example, using observational analyses Reed and Albright (1986) and Gyakum and Danielson (2000) hypothesized that the large surface heat and moisture fluxes well in advance of developing Pacific cyclones, and before the rapid deepening stage, preconditioned the near-surface environment to the extent that explosive deepening occurred. Using an adjoint model on an idealized maritime cyclone, Langland et al. (1995) showed that surface sensible heat fluxes in the warm sector just ahead of the cold front produced the main impact on the cyclone evolution (Fig. 8). Presumably, this was because the low-level jet (LLJ) ahead of the surface cold front is a principal means of inflow to developing cyclones (Wernli 1997). In Langland et al's case, H_s is negative (from the air towards the surface), as can often be the case in cyclone warm sectors, so an increase of C_H (an increase in the magnitude of H_s) would remove heat from the atmosphere and hence be anticyclogenetic. Clearly, the degree to which surface sensible heat and moisture fluxes affect storm evolution and precipitation depends on the location and timing of these fluxes relative to the cyclone and its associated structures. In addition, the magnitude and even the sign of the impact depends on the relative temperatures of the ocean and the atmosphere.

5. Front-relative Flux Locations

Since thermodynamic and kinematic atmospheric conditions vary systematically within extratropical cyclones, and, to some extent, the surface wave characteristics also vary systematically, the surface fluxes vary systematically as well. In order to illustrate the relationship between the surface layer and the synoptic atmospheric environment, Persson et al. (2005a) computed composites of atmospheric surface- layer measurements and ocean surface characteristics along ship paths through 10 storms for which the *R/V Knorr* passed through the open-wave warm sector and the cold front (Figs. 9 and 10). In these composites, time is normalized by the warm sector duration as defined by the low-level moisture and the frontal passage. Negative normalized time is before the frontal passage. These composites and the summary schematic (Fig. 11) show the following:

a) The moistening and warming associated with synoptic-scale advective patterns and surface-layer fluxes lead to minima in the sensible (H_{sc}) and latent (H_{lc}) heat fluxes just before the frontal passage, despite the strong surface winds at this time. Though the warm-sector H_{sc} minimum is slightly negative, the sum of the two heat fluxes is positive, suggesting a positive impact on the synoptic development of these systems.

b) The stress (τ_{sc}) is a maximum just before the frontal passage during the peak in wind speed associated with the warm-sector low-level jet. A second stress maximum of comparable magnitude occurs in the middle of the post-frontal regime. The patterns of heat and momentum fluxes should affect the surface potential vorticity generation, and have dynamical implications for the stability of the frontal zone for frontal wave development.

c) Wave heights increase steadily from the eastern half of the warm sector to the frontal passage, remaining high through most of the post-frontal regime before decreasing.

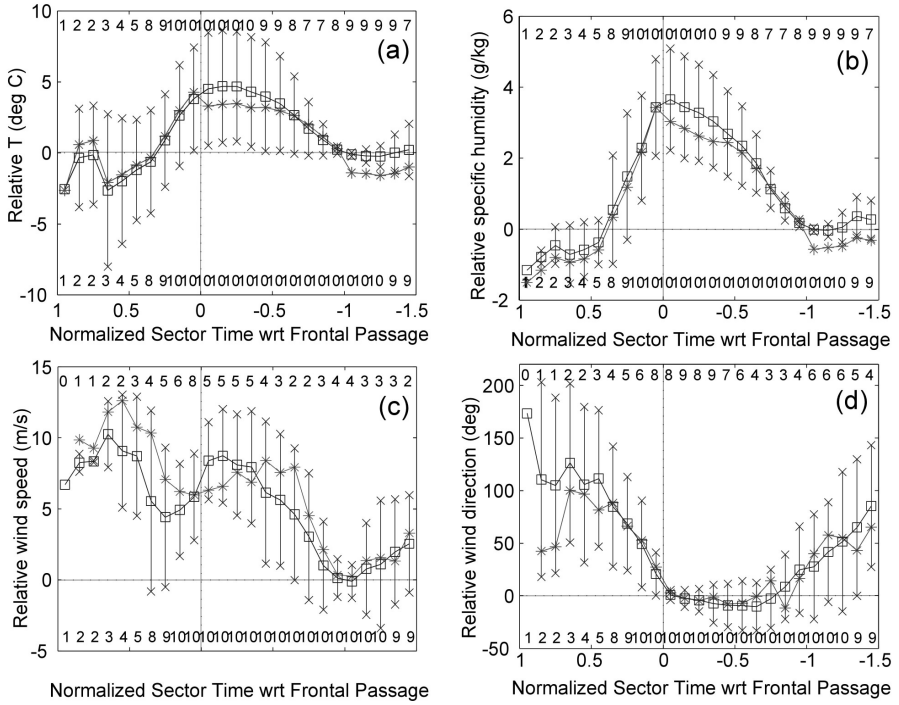

Figure 9. Composite relative values of (a) temperature, (b) specific humidity, (c) wind speed, and (d) wind direction with respect to the cold frontal passage from the R/V Knorr. Values are relative to their values at the onset of the warm sector, except for wind direction, which is relative to the value 1 hour before frontal passage. The stars show the data from the ETL sensors and the squares those from the ship's Athena data system. The 'x's show ±1 standard deviation of the Athena data. The number of cases that contributed to each composite bin for the ETL and Athena sensors are marked at the top and bottom, respectively. (From Persson et al 2005a)

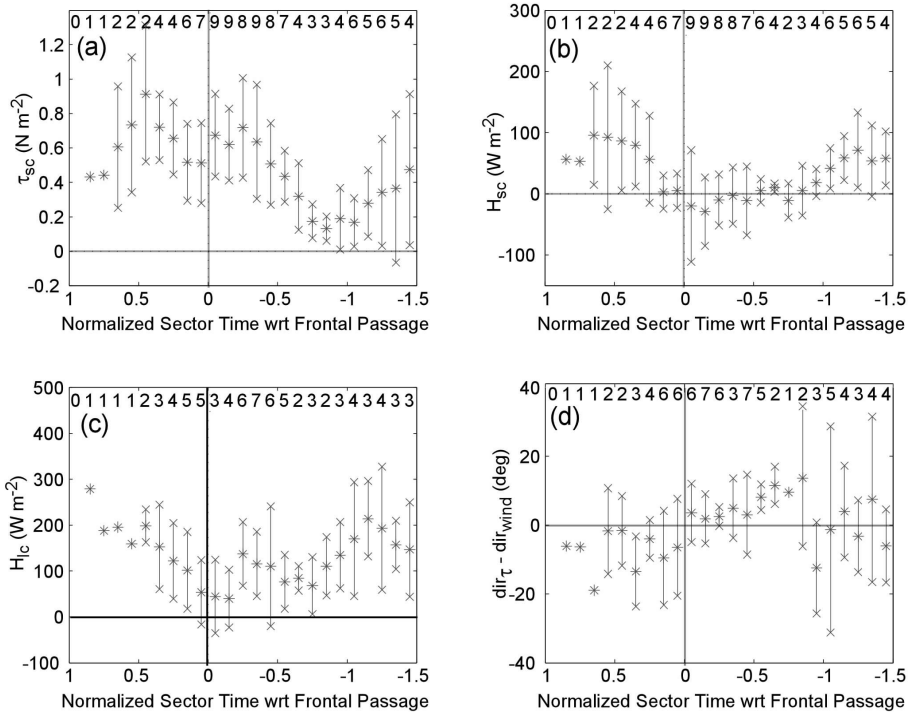

Figure 10. Composite values of (a) stress, (b) sensible heat flux, and (c) latent heat flux determined from the covariance method with respect to the cold frontal passage from the R/V Knorr. Panel (d) shows the composite of the difference between the stress direction and wind direction. A 3-point running mean was applied to the stress components before the stress direction was calculated. The vertical errors bars show ± one standard deviation. (From Persson et al 2005a)

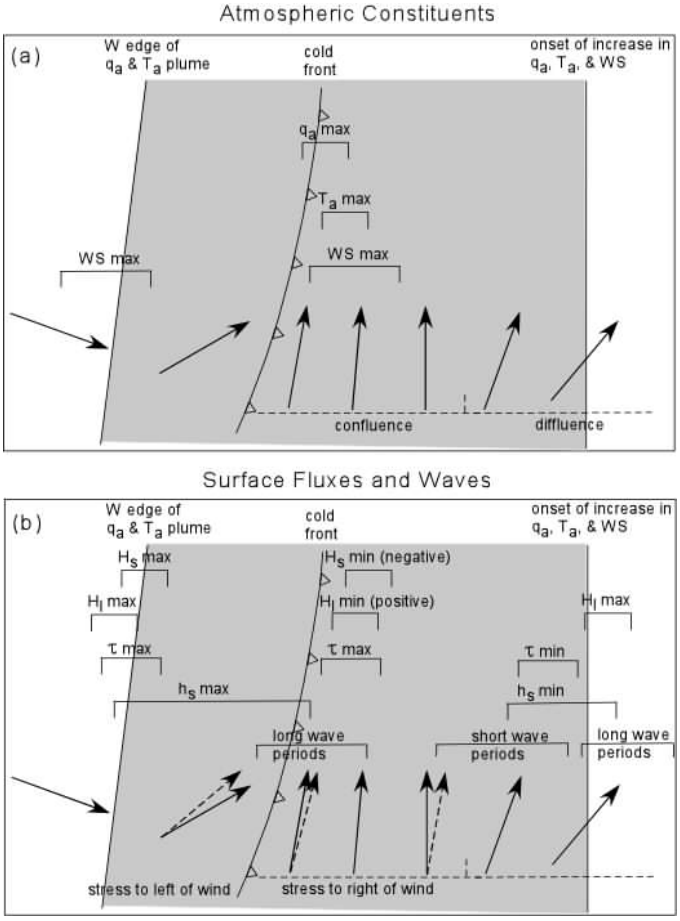

Figure 11: Schematic diagram summarizing the composite variations of (a) the atmospheric constituents, and (b) the surface fluxes and ocean waves relative to the warm sector, cold front, and post-frontal regions. T_a, q_a, WS, H_s, H_l, τ, and h_s represent atmospheric temperature, atmospheric water vapor, wind speed, sensible heat flux, latent heat flux, stress, and significant wave height, respectively. The solid arrows show wind direction and the dashed arrows in (b) show stress direction. The region representing the atmospheric water vapor plume is shaded. (From Persson et al 2005a)

6. Impact of Spatially and Temporally Varying Ocean Characteristics

The sea surface temperature (SST) varies spatially and temporally, with a change time scale of a few days to years. Hence, storms of comparable magnitude and thermal characteristics will be impacted differently over different oceanic regions at different times. Storms passing over the relatively high SSTs of the Gulf Stream in the western Atlantic Ocean will be enhanced to a much greater extent than a similar storm occurring over the relatively cooler waters off the west coast of the United States. Storms impacting the U.S. West Coast are affected differently by the relatively warmer coastal waters during ENSO years compared to non-ENSO years (Persson et al. 2005a). Storms crossing the sharp Gulf Stream SST gradient in the North Atlantic are affected differently than if the sharp SST gradient didn't exist (Giordani and Caniaux 2001).

Furthermore, some of the spatial and temporal variations of the sea surface characteristics are produced by the cyclone itself. Sea surface roughness and sea spray vary spatially, and often systematically, within an extratropical cyclone depending on the wind conditions and the evolutionary history of the storm (Doyle 1995; Perrie et al. 2005; Zhang et al. 2006). These surface characteristic changes can produce important surface flux feedbacks that significantly alter the evolution of the cyclone. Some cyclone-induced variability in SST is also likely, though this feedback has only been studied for tropical cyclones (e.g., Hodur 1997; Bao et al. 2000). This section presents examples of the impact of spatially and temporally variable surface characteristics on surface fluxes and the associated extratropical cyclones.

6.1. Wave characteristics

6.1.1. Surface roughness (wave height and age)

Using a simulation of an idealized extratropical cyclone, Doyle (1995) showed that the frictional effects of wind-generated ocean waves, described in terms of both wave height and wave age, can influence the boundary-layer structure in the vicinity of a marine cyclone. The WAM wave model (WAMDI group 1988) used in connection with the Navy COAMPS model (Hodur 1997) produced maximum significant wave heights in excess of 12 m, with wave height maxima found near the warm front, along the cold front, and to the SW of the cyclone where the wind speeds are the strongest. Because of the translation of the cyclone and the rapidly changing surface winds, the ocean waves are relatively young and growing, producing significant air-sea coupling. Hence, the young waves significantly increase the effective roughness and the surface stress in these areas (Fig. 12), reducing the lowest model level winds by 12-20% compared to simulations where the age of the waves or the change in surface roughness are not considered.

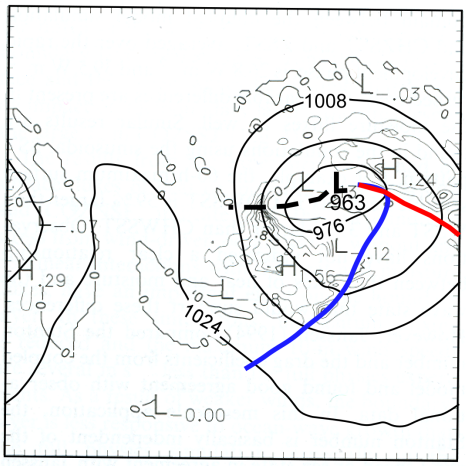

Figure 12: Change in z_0 between the wave model coupled (COZSST) and the uncoupled (CHZSST) simulations (grey; isopleth interval of 0.2 x 10^{-2} m.) The cold front (blue), warm front (red), and post-frontal trough (dashed) are estimated from the surface pressure field (solid, black). Adapted from Doyle (1995).

Because of an increase in τ and despite the decrease in wind speed, surface sensible and latent heat fluxes in the more unstable SW quadrant of the cyclone increased by 30-60% at times. Hence, localized regions of increased TKE and eddy mixing coefficients increase vertical transport of heat, momentum, and moisture. The response of the cyclone central pressure to the frictional changes is complex and can vary by as much as 8-10 mb. The roughness effects of the ocean waves appear at times, to augment the filling of the cyclone. Mesoscale structures, such as the local pressure gradient near the cyclone center, appear to be sensitive to the presence of young ocean waves, and the low-level frontal strength is intensified in localized regions along the warm and cold fronts.

Using the WW3 wave model (Tolman and Chalikov 1996; Tolman 2002) in combination with the Canadian atmospheric MC2 model (Benoit et al. 1997), Zhang et al. (2006) showed that wind-generated ocean waves with wave age considerations will increase the central pressure of strong western Atlantic cyclones by 2-4 mb after 24-36 h of integration and reduce the areal averaged maximum wind speeds by 1.5-2.5 m s^{-1} (~10%) (Fig. 13). These changes in pressure and wind speed occur primarily in the warm sector and to the S and SW of the cyclone (Fig. 14), similar to that found by Doyle (1995). The impact on the storm tracks, however, was small. They found that the wave drag induced friction-related convergence and an enhanced updraft near the cyclone center, with enhanced compensating downdrafts outside the storm center (Fig. 15). Though the vertical motion enhancements were weak (2-3 cm s^{-1}), they increased the static stability, suppressed

convection, and reduced storm intensity. Hence, surface stress impacts propagated to upper levels of the cyclone, as suggested by Doyle (1995).

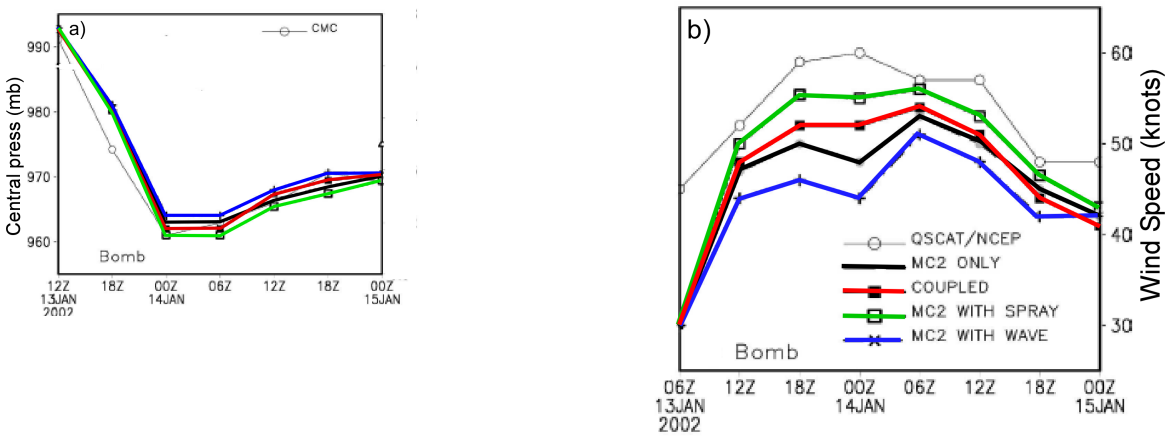

Figure 13: a) Minimum central pressure and b) 200 km2 areal average 10-m winds for the case 'Bomb' using the control MC2 model (heavy black), the coupled wave model (blue), the coupled sea-spray model (green), and full coupling (red). From Zhang et al (2006).

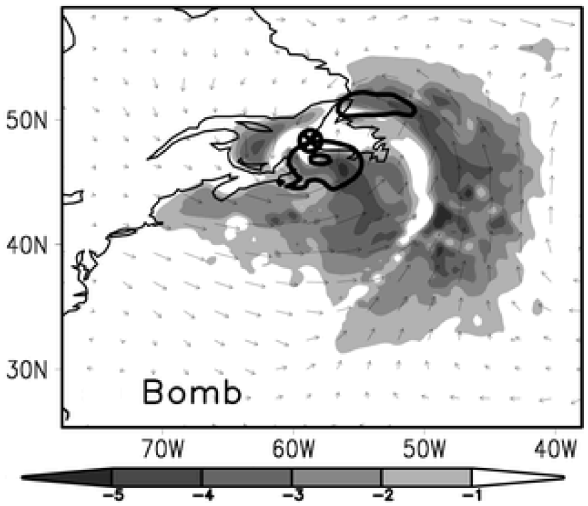

Figure 14. Differences ΔSLP (hPa; contour) and ΔU_{10} (m s^{-1}; shaded) at 'bomb's' peak intensity (0600 UTC 14 Jan 2002) for MC2-wave minus control. ΔSLP contour starts at +1 mb, with intervals at +1 mb. Simulation winds U10 with spray are superposed. Storm center (cross-filled circle) is shown. (From Zhang et al. 2006)

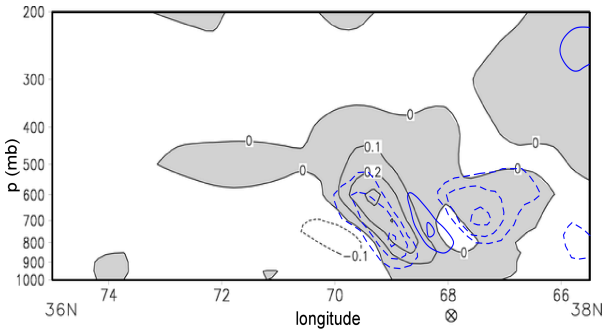

Figure 15. Vertical motion (m s^{-1}) from MC2-only control (black lines) and the difference between MC2-wave minus MC2-only simulations (blue lines). Negative (dashed) is descending motion. Blue isopleth interval is 1 cm s^{-1}, with the 0 cm s^{-1} isopleth omitted. The time is 0600 UTC 21 Jan 2000 when winds and latent heat flux are maximal. The transect line is shown in Fig. 19a. The ringed 'X' shows the circulation center. (Adapted from Zhang et al 2006)

6.1.2. Stress-wind direction mismatch

Differences between the stress and wind directions are suggested to result from either vertical momentum transport by large eddies in a directionally-sheared, baroclinic environment (Geernaert 1988) or from stress effects from sea swell that is oriented differently than the local wind direction (Geernaert et al. 1993; Rieder et al. 1994; Grachev et al. 2003). These two mechanisms are schematically represented in Fig. 16. Because of the effect of vertical shear, the first mechanism would produce stress directions that are oriented to the right of the wind direction (looking downwind and down-stress) in situations of warm-air advection and to the left for cold-air advection. Geernaert (1988) shows how this directional difference changes sign as a warm front and a cold front passes an instrumented North Sea platform.

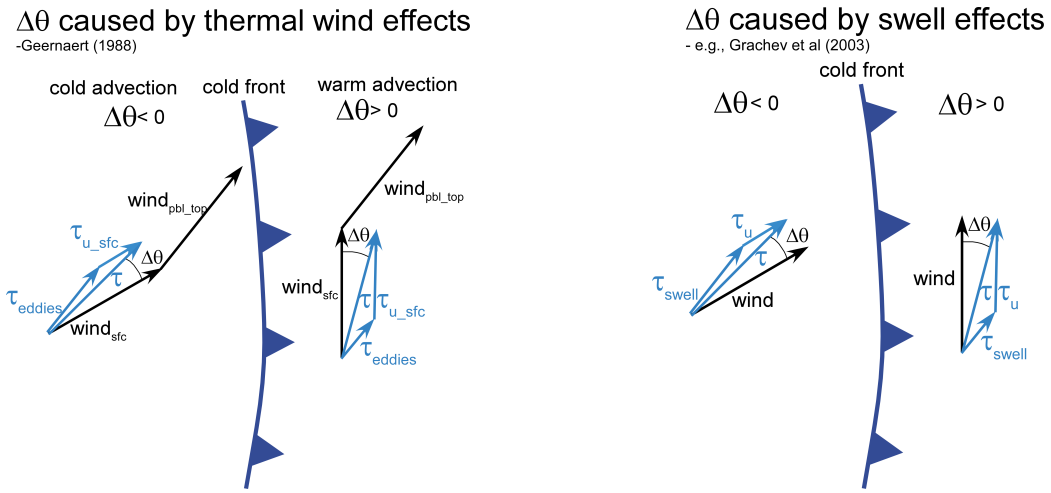

Figure 16: Schematics showing how the observed stress (τ) and wind directional differences (Δθ) across a cold front can result from a) swell effects and b) thermal wind effects.

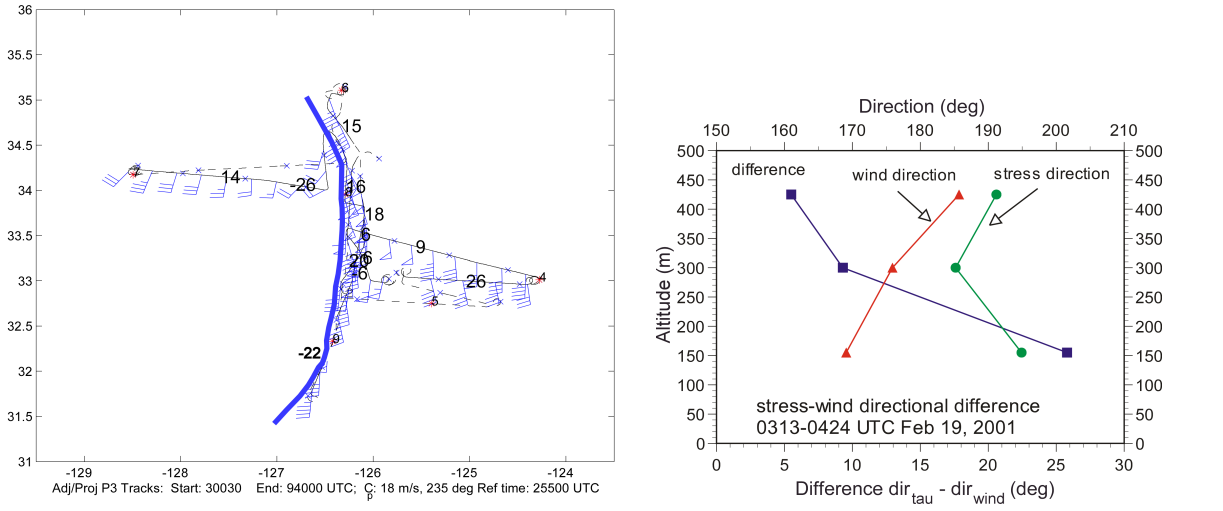

Figure 17 a) Time-to-space adjusted flight track (black lines) and wind barbs (plotted every 4 minutes) for flight legs below 500 m on Feb. 19, 2001, by the NOAA P-3 aircraft over the eastern Pacific Ocean. Latitude and longitude are shown on the vertical and horizontal axes. The difference between the stress direction calculated from the aircraft gust probe data and the aircraft wind direction are shown in bold for 5-10 minute flux legs below 500 m altitude. Positive values indicate a more clockwise orientation of the stress vector. The heavy blue line marks the approximate location of the surface cold front, and dashed flight track indicates altitudes above 500 m. b) Vertical profiles of wind direction, stress direction and directional difference in the warm sector of the storm of Feb. 19, 2001, from NOAA P-3 aircraft measurements. (Panel a) is from Persson et al. 2004).

In the second mechanism, stress effects from swells affect the part of the wind covariance spectrum associated with the swell frequencies (Geernaert et al. 1993; Rieder et al. 1994), producing a net stress direction between the wind direction and the swell direction. Grachev et al. (2003) shows that the wind stress is a vector sum of the 1) pure shear stress aligned with the mean wind shear, 2) wind-wave-induced stress aligned with the direction of the pure wind-sea waves, and 3) swell-induced stress aligned with the swell direction. The swell and wind directions may become different in the vicinity of atmospheric fronts as the swell orientations change much less or more slowly than does the wind direction. Physically, this may result either because the swells move faster than the cold front so post-frontal swell orientations are found ahead of the cold front, or because a cold front moves fast enough to not influence the swells over a long enough time period to change their orientation to that of the winds.

Both the baroclinic effects and the swell effects may lead to different orientations of the wind and stress directions near atmospheric fronts, and both mechanisms should produce a systematic change in the sign of this difference from one side of the front to the other. Evidence for the systematic change can be seen in the stress-wind directional differences composited for the 10 FASTEX cold-frontal cases (Persson et al. 2005a; Fig. 9d) and in the low-level aircraft measurements on both sides of a strong cold front over the eastern Pacific Ocean (Persson et al. 2004; Fig. 17a). The FASTEX composites show that the stress direction is greater than the wind direction by 5-12° (that is, the stress direction is to the right of the wind direction) in the central and western portion of the warm sector east of the surface cold front, while in the post-frontal regime the opposite appears to be true. Manual observations of the swell direction during FASTEX show that the warm sector stress direction is frequently between the swell direction and the wind direction, in qualitative agreement with theory. For the Pacific Ocean case, stress directions 150-200 m above the surface were oriented between 6° and 26° to the right of the wind direction east of the cold front while they were up to 26° to the left of the wind direction west of the cold front. The aircraft measurements also showed that this stress-wind directional difference decreases with height (Fig. 17b). Since both mechanisms should produce larger differences near the surface than aloft, this vertical decrease only supports that one (or both) of these mechanisms is (are) producing the observed directional differences, but can not be used to differentiate between the mechanisms.

The presence of the systematic directional differences between stress and wind implies that flux parameterizations, especially for stress, may need to consider the directional aspects in the vicinity of frontal zones. Furthermore, satellite-based scatterometer wind directions, which rely on the surface stress field, will be in error and will underestimate the surface directional wind shift across the front. Thus the derivative fields, such as convergence and vorticity, will also be underestimated (Persson et al. 2004).

6.2. Sea spray

Sea spray can contribute to both the sensible and latent heat flux during high wind conditions. When spray droplets are injected into the droplet evaporation layer, typically extending one significant wave height above mean sea level, they have the same temperature as the sea water and a broad size spectrum. During their flight before falling back into the water, the droplets' temperature evolves towards an equilibrium temperature and the size towards an equilibrium radius (Andreas et al. 1995; Andreas and DeCosmo 1999, 2002) that are dependent on the salinity, the initial radius, the relative humidity, and initial temperature. However, the transfer of sensible heat from the droplet to the atmosphere occurs much faster than the transfer of moisture. Because most drops of appreciable size have short suspension times, spray sensible heat flux is therefore the primary route by which spray affects storm energy (Andreas and Emanuel 2001; Andreas et al. 2008). Spray latent heat flux is only a small positive feedback term that arises because the evaporating spray cools the near-surface air and thereby enhances the air-sea temperature difference.

Andreas (1995) devised a full microphysical spray model describing this evolution, though it is too complicated to be included in a three-dimensional atmospheric model. Perrie et al. (2005) and Zhang et al. (2006) incorporated a simplified version into the Canadian community model (MC2), the key assumptions being that only droplets of one radius contribute the bulk of the sensible heat and moisture fluxes and that the spray generation can be modeled using an empirical wind function that is dependent on friction velocity, u*. A newer version with updated wind functions based on HEXOS and FASTEX data has recently been published (Andreas et al. 2008) but not yet tried in a 3-D atmospheric model. These parameterizations assume that the total sensible ($H_{s,T}$) and latent ($H_{l,T}$) heat fluxes are computed from the sum of the interfacial fluxes (H_s and H_l) and that contributed from the sea spray:

$$H_{s,T} = H_s + Q_{s,sp} \tag{2}$$

$$H_{l,T} = H_l + Q_{l,sp} , \tag{3}$$

where $Q_{s,sp}$ and $Q_{l,sp}$ are the sea-spray contributed sensible and latent heat fluxes. $Q_{s,sp}$ depends on the SST, the droplet equilibrium temperature for droplets of radius 100 μ ($T_{eq.100}$), and the sensible heat wind function; $Q_{l,sp}$ depends on the equilibrium radius for droplets of radius 50 μ ($r_{eq.50}$), the droplet lifetime ($\tau_{r,50}$), the significant wave height ($H_{1/3}$), and the latent heat wind function. The approximations reported in Andreas (2005a) provide the necessary microphysical variables $T_{eq.100}$, $r_{eq.50}$, and $\tau_{r,50}$.

Perrie et al. (2005) and Zhang et al. (2006) evaluated the impact of including the sea spray effects (using the older parameterization version) on the evolution of three strong extratropical cyclones along the east coast of North America. The impact on the tracks of the cyclone centers was small. However, the sea spray produced decreases in surface pressure of a few millibars and increases in the surface wind of a few meters per second (Fig. 13), especially in the warm sector ahead of the surface cold front and to the S and W of the cyclone center (Fig. 18). The sea-spray effect on the surface pressure and near-surface winds are opposite in sign to those of the wave drag (compare to Fig. 14) but comparable in magnitude and affect similar regions of the cyclone. The sea-spray effects were apparently caused by increases of 100-700 W m^{-2} in the total heat flux in the warm sector ahead of the cold front and in the bent-back portions of the circulation to the SW and S of the low center (Fig. 19a). The model results showed that the latent heat fluxes were impacted more than the sensible heat fluxes (Fig. 20), despite the theoretical expectation to the contrary. This may be due to storm

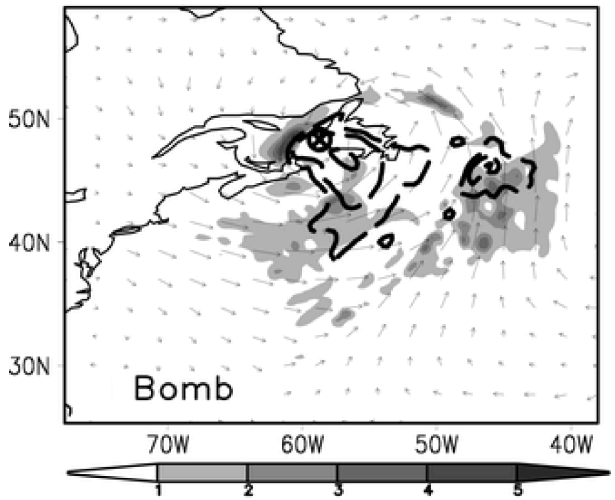

Figure 18: Differences ΔSLP (hPa; contour) and ΔU_{10} (m s^{-1}; shaded) at bomb's peak intensity (0600 UTC 14 Jan 2002) MC2-spray minus control. ΔSLP contour starts at −1 mb, with intervals at −1 mb. Simulation winds U_{10} with spray are superposed. Storm center (cross-filled circle) is shown. (From Zhang et al. 2006)

intensification feedbacks not directly included in the parameterization, though this issue needs to be explored further. Despite the similar magnitudes but opposite signs in effect when considered individually, when both sea-spray and wave drag are realistically included, the changes due to sea-spray seem to dominate during the first 30 h of the 42 h simulation, though the wave drag had the larger effect during the dissipation stages of the cyclones (Figs. 13, 19b and 20).

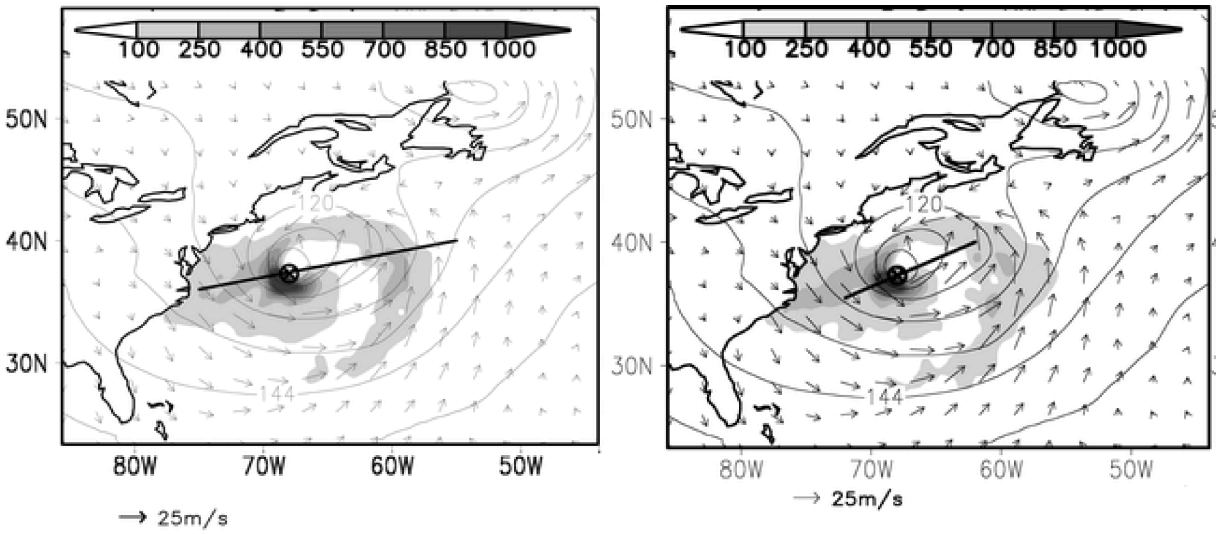

Figure 19: Total heat flux difference (ΔSH + ΔLH; shaded areas; W m^{-2}) for a) MC2-spray minus MC2-only control simulations at 0600 UTC 21 Jan 2000 (superbomb), superposed with control simulation of heights at 850 hPa (thin solid lines) and wind speed at 1000 hPa and b) the fully coupled and control simulation (MC2-wave-spray minus MC2 only) for the superbomb at 0600 UTC 21 Jan 2000. Transect sections go through the storm center and the high-wind region, as indicated by solid black lines. (Zhang et al 2006)

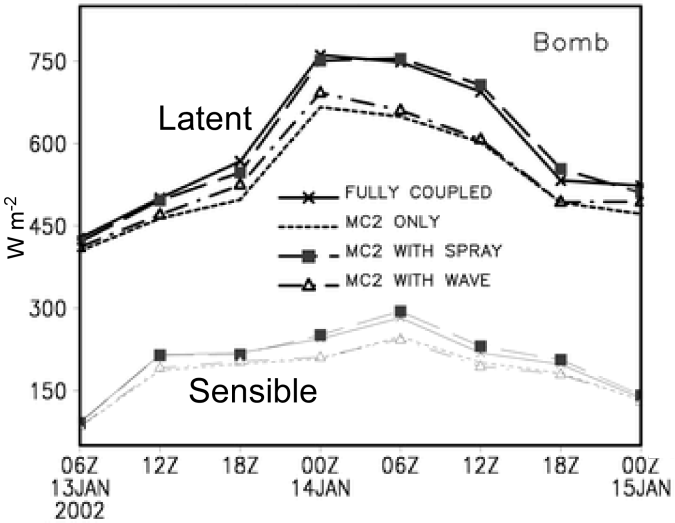

Figure 20: Time series for 200 × 200 km^2 area-averaged sensible (bottom four plotted time series) and latent (top four plotted time series) following maximal flux center storm with and without spray and waves for the bomb. (From Zhang et al. 2006)

6.3. Sea-surface temperature

In Fig. 8, H_s suppressed the cyclone evolution because fluxes were downward due to the relatively warm southerly flow in the LLJ region passing over cooler waters typical of the North Pacific Ocean. In the simulations of Kuo et al. (1991), the warm sea-surface temperatures (SSTs) of the Gulf Stream in the western Atlantic Ocean moistened and warmed the relatively cool air flowing out from the North American continent, enhancing the development of the cyclones and their attendant precipitation. Hence, storms of comparable magnitude and thermal characteristics will be impacted differently over different oceanic regions.

In an extreme case, Giordani and Caniaux (2001) showed that significant changes occurred in a developing, open-ocean storm passing over the strong 12°C SST gradient in the northwest Atlantic Ocean. Within 7 hours of entering the warmer waters, the central pressure of the simulated storm was 11 mb deeper when compared to a simulation with spatially constant cold SSTs, and the track of the low deviated as well. In addition, the total precipitation in the case with the SST gradient was 66% greater, which was in large part due to the nearly threefold increase in the convective precipitation. These significant differences were due to the replacement of the significant downward sensible and latent heat flux in the warm sector with a near-zero heat flux and the increase in the baroclinicity due to an increase in the warm air advection as the storm entered the warmer waters in the case with the SST gradient.

The effects of coastal surface heat fluxes, modulated by less extreme temporal and regional variability of SSTs, on frontal precipitation is shown by Persson et al. (2005b). Aircraft measurements of offshore and nearshore surface fluxes (H_s =12 Wm^{-2}; Hl = 32 Wm^{-2}) and boundary-layer structure in the warm-sector just ahead of a cold front showed that the observed approximately 1 K change in boundary-layer θ_e can be accounted for by the surface fluxes along the 2.5 h (140 km) path of the boundary-layer air parcel towards the coast (Figs. 21 and 22). This 1 K increase of boundary layer θ_e increases the CAPE by about 26% from 391 J kg^{-1} to 491 J kg^{-1}. Furthermore, calculations show that this energy flux is also sufficient to account for the observed decrease in the level of free convection (z_{LFC}) from 1060 m offshore to 550 m nearshore. This latter point is important, as the abrupt rise of the cold front offshore was only 700 m, apparently too low to allow the warm sector air to reach the local z_{LFC} through forced lifting by the cold front, as is suggested by the lack of convection at the offshore cross section. However, closer to the coast, the air did reach the z_{LFC} and additional CAPE was available, producing convection reaching to 6.5 km and heavy coastal precipitation and local flooding. The CAPE calculations and the associated changes in z_{LFC} show that the coastal surface fluxes significantly decrease the stability, thereby contributing to the offshore extent and intensity of the very heavy, but brief, precipitation observed along this part of the California coast. Though the coastal surface fluxes are not the primary cause for the coastal convection, their significant contribution to the destabilization will produce a positive contribution to the convection.

Reasonable values of H_s, H_l and the resultant 2.5 h change in θ_e were obtained from the COARE 3.0 flux scheme using the observed environmental conditions in the coastal zone, including the observed low-level winds, air temperature, boundary-layer depth, and SSTs (Fig. 23). However, because these measurements were made during the El Niño conditions of February 1998, the coastal SSTs were anomalously high by about 2°C.

For SSTs 1.5°–2.0°C cooler than those observed, representative of non–El Niño years, the H_s was substantially negative (-15 to -20 W m^{-2}) and the H_l was positive (10-22 W m^{-2}) but smaller. Hence, the change in θ_e is predicted to be near zero or slightly negative. That is, coastal surface fluxes would not be expected to contribute to the destabilization of the boundary layer during an identical landfalling storm in a

non–El Niño year, even though they do contribute during El Niño years. They might even lead to slight stabilization.

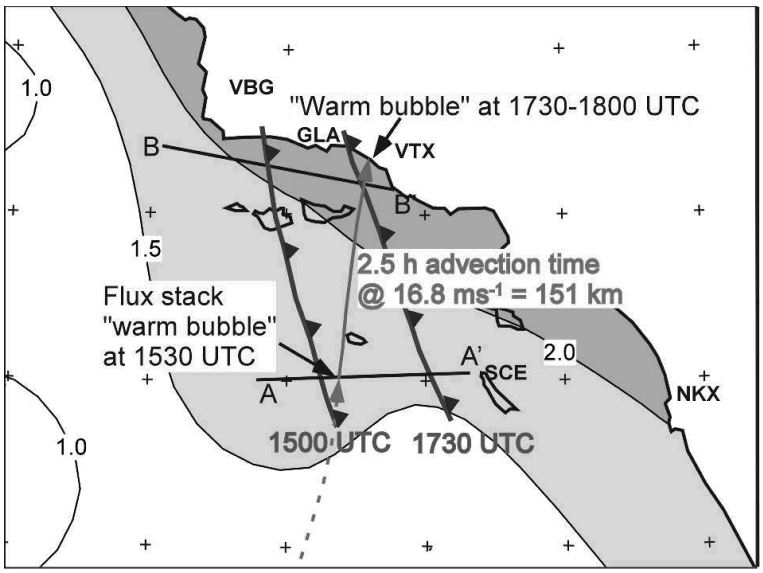

Figure 21: Schematic of the parcel trajectory from the offshore cross section (A–A') to the nearshore cross section (B–B') at the north coast of the California Bight. The two heavy lines with frontal symbols represent the secondary cold front at 1500 and 1730 UTC, respectively. The isopleths show the SST anomaly (°C) for 2 Feb 1998, with the anomalies above +1.5°C (light shading) and +2.0°C (dark shading) highlighted. (From Persson et al. 2005b)

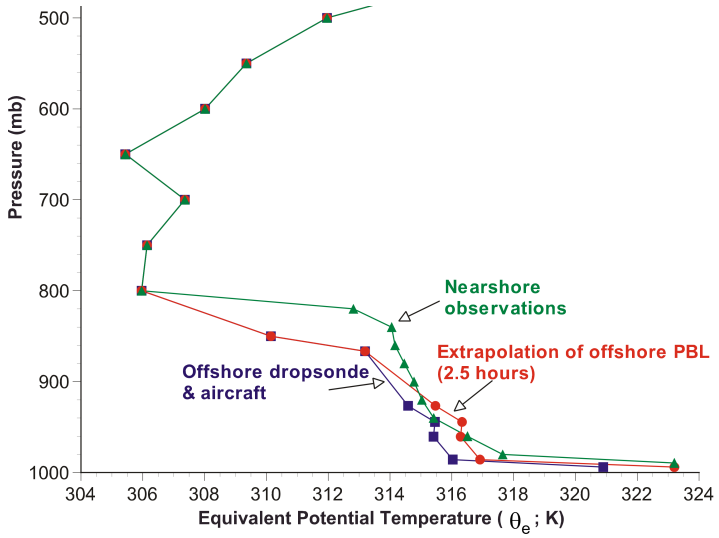

Figure 22: Profiles of equivalent potential temperature (θ_e) for the offshore location (squares), extrapolation to the nearshore location using boundary layer changes due only to surface fluxes (dots), and nearshore observations (triangles). The offshore dropsonde data are used above the aircraft data for all profiles, i.e., above 867 mb for the offshore and extrapolated offshore profiles and above 820 mb for the observed nearshore profile. The 1200 UTC Vandenberg sounding is used above 500 mb. (From Persson et al. 2005b)

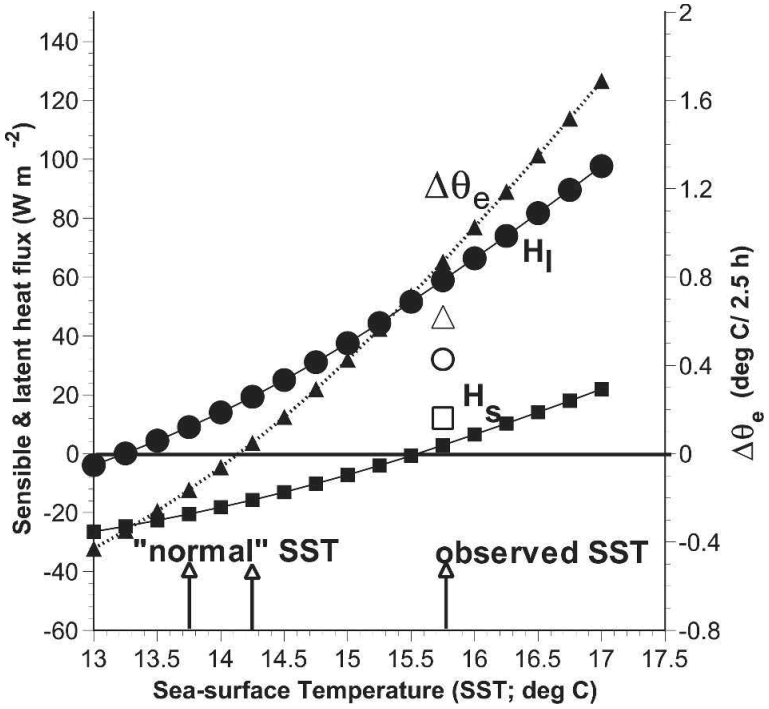

Figure 23: Sensible heat flux (H_s; solid squares), latent heat flux (H_l; solid circles), and associated 2.5-h change in the boundary layer θ_e ($\Delta\theta_e$; solid triangles) as a function of SST. The computations of H_s, H_l, and $\Delta\theta_e$ were done using the bulk algorithm of Fairall et al. (2003) and assuming conditions as observed in the offshore warm sector on 3 Feb (given by the flight leg at 66 m, and with PBL height ~ 600 m). Also shown are the observed covariance H_s (open square), H_l (open circle), and $\Delta\theta_e$ (open triangle). The observed SST and the range from more normal years are marked by arrows along the bottom. (From Persson et al. 2005b)

Usually, the modulation of California precipitation by ENSO is discussed in a larger-scale context, where large-scale connections with tropical regions have modified the atmospheric circulation over the Pacific Ocean allowing more and stronger storms to impact California. The ENSO-modulated physical mechanism presented here appears therefore not to have been previously considered. Through an enhancement of CAPE during pre-cold-frontal onshore flow, this mechanism links the generation of anomalously warm SSTs along the California coast to small but potentially significant enhancements in the coastal cold-frontal precipitation from each storm, thereby adding to the ENSO-enhanced precipitation in that region. This case only serves as a suggestion that this process may contribute to coastal precipitation. Studies using more cases and producing boundary layer mean states for El Niño and non–El Niño years are necessary to assess the climatological importance of this process. Though the connection is speculative, this case provides a specific example of how the surface-flux modulation of an extratropical cyclone interacts with the El Niño modulation of the coastal SST anomalies to impact individual storms and thereby the coastal climate.

7. Summary and Suggestions for Future Work

The timing and location of the surface sensible and latent heat fluxes and momentum fluxes with respect to the evolution and key structures of mid-latitude cyclones determine their impact on the cyclones. Surface sensible and latent heat fluxes impact the intensity of a developing mid-latitude cyclone most if they occur before the rapid deepening phase. Storm intensity is most sensitive to sensible and latent heat fluxes occurring in the warm sector, and perhaps near the surface warm front. Sensitivity tests suggest that storm track and intensity are more sensitive to the way the surface fluxes are distributed in the vertical by PBL schemes than to the magnitude differences between commonly used surface flux parameterizations, though additional studies are needed to more quantitatively separate these effects. However, intensity sensitivity to

the surface fluxes themselves is clearly illustrated by the impacts of the inclusion of coupled wave models and sea-spray representations. Wave drag effects tend to decrease the near-surface winds by a few meters per second and usually, but not always, tend to increase the storm's central pressure by a few millibars. Recent studies with sea-spray effects suggest that they will increase extratropical storm intensity (increase winds, decrease central pressure) by magnitudes comparable to the effects of wave drag. Largest increases in sensible and latent heat flux occur in the favored warm sector and SW quadrant regions of the storms, with increased fluxes in the former region perhaps having the more important impact. Interestingly, when wave drag and sea-spray effects are both included, the results are similar to the effects of just sea spray.

Spatial variability of sea-surface temperature can also impact the evolution of mid-latitude cyclones and the resulting precipitation, as documented for the SST gradients associated with the North Atlantic Gulf Stream and the California coastal current. Effects of temporal variability of SSTs have been suggested for those occurring with slower-evolving phenomenon such as ENSO. No studies have been done of the feedback effects of the more rapid SST changes possibly occurring with deep mid-latitude cyclones themselves, though such effects have been found important for tropical hurricanes.

Future work should focus on a better understanding of impacts of the spatially and temporally variable surface characteristics. For instance, a clearer elucidation is necessary of the sensitivity of cyclone evolution and structure to the location of surface fluxes relative to the frontal features and cyclone life cycle stage. Also, sensitivity studies that separate the impacts of the surface flux interfacial schemes from the PBL schemes are needed. The use of more sophisticated modeling techniques or dynamically important diagnostic parameters, such as adjoint models and potential vorticity, may be necessary. The incorporation of the best off-line flux schemes into the three-dimensional models should be encouraged. If the full atmospheric model results suggest that surface flux parameterization improvements are needed, additional off-line tests of surface flux schemes that include more sea-surface characteristics, such as wave characteristics, sea-spray, and stress-wind mismatch, should be done. To facilitate off-line tests, additional measurements in high-wind conditions associated with mid-latitude cyclones are needed, where the storm-relative environment is documented. Studies of impacts of aerosol fluxes (e.g., sea salt) on extratropical cyclone microphysics and evolution, of which there may be some, will require the use of models such as the WRF/Chem model (Grell et al. 2005)

Only the impacts of a liquid ocean surface have been considered here. Surface flux changes and their impacts on polar low development have been studied for flow from the sea ice to the open ocean. Very little has been done to evaluate the impact of surface flux changes as extratropical cyclones move from open water to over the sea ice. This is potentially important for understanding how extratropical cyclones impact the disappearing sea ice and as the Arctic Ocean includes more open water.

8. References

Andreas, E. L, 1995: The temperature of evaporating sea spray droplets. *J. Atmos. Sci.*, **52**, 852–862.

____, 2005: Approximation formulas for the microphysical properties of saline droplets. *Atmos. Res.*, **75**, 323–345.

____, and J. DeCosmo, 1999: Sea spray production and influence on air-sea heat and moisture fluxes over the open ocean. *Air-Sea Exchange: Physics, Chemistry and Dynamics*, G. L. Geernaert, Ed., Kluwer, 327–362.

____, and , 2002: The signature of sea spray in the HEXOS turbulent heat flux data. *Bound.-Layer Meteor.*, **103**, 303–333.

____, J. B. Edson, E. C. Monahan, M. P. Rouault, and S. D. Smith, 1995: The spray contribution to net evaporation from the sea: A review of recent progress. *Bound.-Layer Meteor*., **72**, 3–52.

____, and K. A. Emanuel, 2001: Effects of sea spray on tropical cyclone intensity. *J. Atmos. Sci*., **58**, 3741–3751.

____, P. O. G. Persson, and J. E. Hare, 2008: A bulk turbulent air-sea flux algorithm for high-wind, spray conditions. *J. Phys. Ocean*, **38**, 1581-1596.

Anthes, R. A., E.-Y. Hsie, and Y.-H. Kuo, 1987: Description of the Penn State/NCAR Mesoscale Model Version 4 (MM4). *NCAR Tech. Note, NCAR/TN-282+STR*, 66 pp.

Bao, J.-W., J. M. Wilczak, J-K Choi,, and L. A. Kantha, 2000: Numerical simulations of air-sea interaction under high wind conditions using a coupled model: a study of hurricane development. *Mon. Wea. Rev*., **128**, 2190-2210.

Beljaars, A. C. M., 1995a: The impact of some aspects of the boundary layer scheme in the ECMWF model. *Proc. Seminar on Parameterization of Sub-Grid Scale Physical Processes*, Reading, ECMWF.

____, 1995b: The parameterization of surface fluxes in large scale models under free convection. *Quart. J. Roy. Meteor. Soc*., **121**, 255–270.

Benoit, R., M. Desgagne, P. Pellerin, Y. Chartier, and S. Desjardins, 1997: The Canadian MC2: A semi-implicit semi-Lagrangian wide-band atmospheric model suited for fine-scale process studies and simulation. *Mon. Wea. Rev*., **125**, 2382-2415.

Blackadar, A. K., 1976: Modeling the nocturnal boundary layer. *Proceedings of the Third Symposium on Atmospheric Turbulence, Diffusion and Air Quality*, pp. 46-49, Amer. Meteor. Soc., Boston, Mass.

____, 1979: High resolution models of the planetary boundary layer. *Advances in Environmental Science and Engineering*. No. 1. Pfafflin and Ziegler, Eds., Gordon and Breach, 50-85.

Brunke, M. A., C. W. Fairall, X. Zeng, L. Eymard, and J. A. Curry, 2003: Which bulk aerodynamic algorithms are least problematic in computing ocean surface turbulent fluxes? *J. Climate*, **16**, 619–635.

Burk, S. D, and W. T. Thompson, 1989: A vertically nested regional numerical prediction model with second-order closure physics. *Mon. Wea. Rev*., **117**, 2305-2324.

Doyle, J. D., 1995: Coupled ocean wave/atmosphere mesoscale model simulations of cyclogenesis. *Tellus*, **47A**, 766-778.

Eymard, L., and Coauthors, 1999: Surface fluxes in the North Atlantic Current during the CATCH/FASTEX experiment. *Quart. J. Roy. Meteor. Soc*., **125**, 3563–3599.

Fairall, C. W., E. F. Bradley, J. E. Hare, A. A. Grachev, and J. B. Edson, 2003: Bulk parameterization of air-sea fluxes: Updates and verification for the COARE algorithm. *J. Climate*, **16**, 571–591.

Geernaert, G. L., 1988: Measurements of the angle between the wind vector and wind stress vector in the surface layer over the North Sea. *J. Geophys. Res*., **93**, 8215-8220.

____, F. Hansen, M. Courtney, and T. Herbers, 1993: Directional attributes of the ocean surface wind stress vector. *J. Geophys. Res*., **98**, 16,571-16,582.

Giordani, H., and G. Caniaux, 2001: Sensitivity of cyclogenesis to sea surface temperature in the northwest Atlantic. *Mon. Wea. Rev*., **129**, 1273-1295.

Grachev, A. A., C. W. Fairall, J. E. Hare, J. B. Edson, and S. D. Miller, 2003: Wind stress vector over ocean waves. *J. Phys. Oceanogr*., **33**, 2408-2429.

Grell, G. A., Y.-H. Kuo, and R. Pasch, 1991: Semiprognostic tests of cumulus parameterization schemes in the middle latitudes. *Mon. Wea. Rev*., **119**, 5-31.

____, J. Dudhia, and D. R. Stauffer, 1994: A description of the fifth-generation Penn State/NCAR Mesoscale Model (MM5). *NCAR Technical Note*, NCAR/TN-398+STR. [Available from NCAR Publication Office, Box 3000, Boulder, CO 80303]

____, S. E. Peckham, R. Schmitz, S. A. McKeen, G. frost, W. C. Skamarock, and B. Eder, 2005: Fully coupled 'online' chemistry within the WRF model. *Atmos. Environ*., **39**, 6957-6975.

Gyakum, J. R., and R. E. Danielson, 2000: Analysis of meteorological precursors to ordinary and explosive cyclogenesis in the western North Pacific. *Mon. Wea. Rev*., **128**, 851-863.

Hodur, R. M., 1997: The Naval Research Laboratory's Coupled Ocean/Atmosphere Mesoscale Prediction System (COAMPS). *Mon. Wea. Rev*., **125**, 1414-1430.

Hong, S.-Y., and H.-L. Pan,1996: Nonlocal boundary layer vertical diffusion in a medium-range forecast model. *Mon. Wea. Rev*., **124**, 2322-2339.

Joly, A., and 24 coauthors, 1999: Overview of the field phase of the Fronts and Atlantic Storm-Track Experiment (FASTEX) project. *Quart. J. Roy. Meteor. Soc*., **125**, 3131-3163.

Kristjánsson, J. E., and S. Thorsteinsson, 1995: The structure and evolution of an explosive cyclone near Iceland. *Tellus*, **47A**, 656-670.

Kuo, Y.-H., and R. J. Reed, 1988: Numerical simulation of an explosively deepening cyclone in the eastern Pacific. *Mon. Wea. Rev*., **116**, 2081-2105.

____, ____, and S. Low-Nam, 1991: Effects of surface energy fluxes during the early development and rapid intensification stages of seven explosive cyclones in the western Atlantic. *Mon. Wea. Rev*., **119**, 457-476.

Langland, R. H., R. L. Elsberry, and R. M. Errico, 1995: Evaluation of physical processes in an idealized extratropical cyclone using adjoint techniques. *Quart. J. Roy. Meteor. Soc*., **121**, 1349-1386.

Liu W. T., K. B. Katsaros, and J. A. Businger, 1979: Bulk parameterization of air–sea exchanges of heat and water vapor including the molecular constraints at the interface. *J. Atmos. Sci*., **36**, 1722–1735.

Louis, J-F., 1979: Parametric model of vertical eddy fluxes in the atmosphere. *Bound.-Layer Meteor*., **17**, 187-202.

Oost, W. A., G. J. Komen, C. M. J. Jacobs, and C. van Oort, 2002: New evidence for a relationbetween wind stress and wave age from measurements during ASGAMAGE. *Boundary-Layer Meteorol*., **103**, 409-438.

Perrie, W., E. L Andreas, W. Zhang, W. Li, J. Gyakum, and R. McTaggart-Cowan, 2005: Sea spray impacts on intensifying midlatitude cyclones. *J. Atmos. Sci*., **62**, 1867-1883.

Persson, P. O. G., J. E. Hare, C. W. Fairall, and William Otto, 2005a: Air-sea interaction processes in warm and cold sectors of extratropical cyclonic storms observed during FASTEX. *Quart. J. Roy. Meteor. Soc*., **131**, 877-912, doi:10.1256/qj.03.181.

____, L. B. Nance, J. E. Hare, and A. White, 2003: Mid-Atlantic frontal wave development, boundary layer structure, and surface fluxes in FASTEX IOP1: Observations and sensitivity experiments. *Preprints, 10th Conf. on Mesoscale Processes*, 23-27 June, Portland, OR. (Paper 1.2 on CD)

____, P. J. Neiman, B. Walter, and M. Ralph, 2005b: Contributions from California coastal-zone surface fluxes to heavy coastal precipitation: A CALJET case study during the strong El Niño of 1998. *Mon. Wea. Rev.*, **133**, 1175-1198.

____, B. Walter, and J. Hare, 2004: Maritime differences between wind direction and stress: Relationships to atmospheric fronts and implications. CD -ROM of Preprints, *16th Symposium on Boundary Layers and Turbulence*, 9-13 Aug, Portland, ME.

Reed, R. J., and M. D. Albright, 1986: A case study of explosive cyclogenesis in the eastern Pacific. *Mon. Wea. Rev.*, **114**, 2297-2319.

____, and W. Blier, 1986a: A case study of comma cloud development in the eastern Pacific. *Mon. Wea. Rev.*, **114**, 1681-1695.

____, and ____, 1986b: A further study of comma cloud development in the eastern Pacific. *Mon. Wea. Rev.*, **114**, 1696-1708.

____, and A. J. Simmons, 1991: An explosively deepening cyclone over the North Atlantic that was unaffected by concurrent surface energy fluxes. *Wea. Forecasting*, **6**, 117-122.

Rieder, K. F, J. A. Smith, and R. A. Weller, 1994: Observed directional characteristics of the wind, wind stress, and surface waves on the open ocean. *J. Geophys. Res.*, **99**, C11, 22,589-22,596.

Shafran, P.C., N.L. Seaman, and G.A. Gayno, 2000: Evaluation of numerical predictions of boundary layer structure during the Lake Michigan Ozone Study (LMOS). *J. Appl. Meteorol.*, **39**, 412-426.

Taylor, P. K., and M. A. Yelland, 2001: The dependence of sea surface roughness on the height and steepness of the waves. *J. Phys. Oceanogr.*, **31**, 572-590.

Tolman, H. L., 2002: Alleviating the garden sprinkler effect in wind wave models. *Ocean Modell.*, **4**, 269-289.

____, and D. V. Chalikov, 1996: Source terms in a third-generation wind wave model. *J. Phys. Oceanogr.*, **26**, 2497-2518.

WAMDI Group (S. Hasselmann, K. Hassellmann, E. Bauer, P. A. E. M. Janssen, G. Komen, L. Bertotti, P. Lionello, A. Guillame, V. Cardone, J. Greenwood, M. reistad, L. Zambresky and J. Ewing), 1988: The WAM model-a third generation ocean wave prediction model. *J. Phys. Oceanogr.*, **18**, 1775-1810.

Wernli, H., 1997: A Lagrangian-based analysis of extratropical cyclones. II: A detailed case-study. *Quart. J. Roy. Meteor. Soc.*, **123**, 1677-1706.

Zhang, D.-L., and R. A. Anthes, 1982: A high-resolution model of the planetary boundary layer-sensitivity tests and comparisons with SESAME-79 data. *J. Appl. Meteor.*, **21**, 1594-1609.

____, E. Radeva, and J. Gyakum, 1999: A family of frontal cyclones over the Western Atlantic Ocean. Part II: Parameter studies. *Mon. Wea. Rev.*, **127**, 1745-1760.

Zhang, W., W. Perrie, and W. Li, 2006: Impacts of waves and sea spray on midlatitude storm structure and intensity. *Mon. Wea. Rev.*, **134**, 2418-2442.